DNS OF VELOCITY AND THERMAL FIELDS IN TURBULENT CHANNEL FLOW WITH TRANSVERSE-RIB ROUGHNESS

Yasutaka Nagano, Hirofumi Hattori, Shin-ya Yasui
Department of Mechanical Engineering,
Nagoya Institute of Technology
Gokiso-cho, Showa-ku, Nagoya 466-8555, Japan
nagano@heat.mech.nitech.ac.jp, hattori@heat.mech.nitech.ac.jp

Tomoya Houra
Department of Environmental Technology,
Nagoya Institute of Technology
Gokiso-cho, Showa-ku, Nagoya 466-8555, Japan
houra@heat.mech.nitech.ac.jp

ABSTRACT

A detailed knowledge of both velocity and thermal fields in wall turbulence disturbed by a row of ribs on the wall is important for clarifying the chief factors of fluid and thermal dynamics related to the control of heat transfer. In this study, in order to elucidate the effects of roughness on the statistical quantities in the velocity and thermal fields, direct numerical simulations (DNS) of heat transfer in turbulent channel flows with transverse-rib roughness are performed by varying their interval, width and height, in which the turbulent heat transfer with k-type and d-type roughness walls are simulated. It is found that since turbulent mixing is promoted by arranging ribs, the distributions of mean velocity and temperature become asymmetric markedly. And the systematic variations of secondary flow patterns between ribs are clearly identified. With the k-type roughness, the best heat transfer performance is found to be obtained.

INTRODUCTION

Arranging roughness elements or protuberances on the heat transfer surface, which is expected to promote near-wall turbulence and improve the efficiency of convective heat transfer, has been applied to many kinds of industrial machinery, including heat exchangers and turbine blades. However, from the standpoint of pump efficiency, these roughness elements have the drawback of causing drag as well as increasing heat transfer. Therefore, a detailed knowledge of both velocity and thermal fields in wall turbulence disturbed by the elements of ribs on the wall is important for clarifying the chief factors of fluid and thermal dynamics related to the control of heat transfer. Experimental investigations for turbulent channel flows with transverse-rib roughness have been reported by numerous researchers (e.g., Hanjalić and Launder, 1972; Antonia and Luxton, 1971, 1972; Perry, 1969). However, it is difficult to measure in detail the characteristics of turbulent flow near the rough wall including transport of heat, because of the lack of detailed information on turbulence structures. On the other hand, the rapid progress in high-performance computers has promoted direct numerical simulation (DNS), which enables us to solve the governing equations as accurately as possible without introducing assumptions. Moreover, DNS serves to increase our understanding of the generation of turbulence and its maintenance mechanisms including the thermal field. Although an analysis has been made of turbulent thermal fields with roughness using DNS (Tsujimoto *et al.*, 2000), there has been no systematic study on the effects of the height and spacing of the roughness elements.

In the present study, to obtain detailed knowledge of the effects of the roughness elements on both velocity and thermal fields in the near-wall region, we performed a DNS using finite difference methods, making it relatively easy to change the boundary conditions. In a DNS, the periodic transverse-rib roughnesses are arranged in the streamwise direction, and the spacing, width and height are varied systematically. The thermal field are thus constructed to simulate so-called k- and d-type roughness. We attempted to obtain the optimal rib arrangement to promote heat transfer, and investigated the turbulence thermal structure from various viewpoints.

NUMERICAL PROCEDURE

Figure 1 shows a schematic channel with transverse-rib roughness and the coordinate system used in the present study. DNS based on the finite-difference method was carried out with a constant mean pressure gradient to balance the wall-shear stress on both walls. The origin of the coordinate axes is located in the middle of the enclosure between the ribs. Table 1 shows the computational methods. The numerical scheme used in this study is validated by comparing the statistical quantities in the plane channel flow with those calculated in our group's DNS (Nagano and Hattori, 2003), which employs the spectral method.

The velocity field is governed by the incompressible Navier-Stokes equation without buoyancy and the continuity equation, which are non-dimensionalized by the mean friction velocity u_{τ_0} at both walls and the channel half width δ. They are given as follows:

$$\frac{\partial u_i^*}{\partial t^*} + u_j^* \frac{\partial u_i^*}{\partial x_j^*} = -\frac{\partial p^*}{\partial x_i^*} + \frac{1}{Re_{\tau_0}} \frac{\partial^2 u_i^*}{\partial x_j^* \partial x_j^*}, \tag{1}$$

$$\frac{\partial u_i^*}{\partial x_i^*} = 0. \tag{2}$$

The boundary conditions for the velocity field are periodic in x and z directions and non-slip on the walls. For the thermal field,

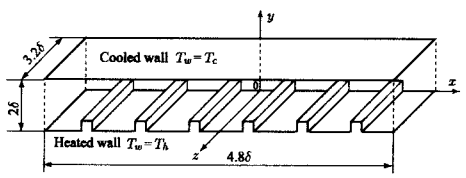

Figure 1: Channel with transverse-rib roughness and coordinate system

Table 1: Computational methods

Channel with transverse-rib roughness		
Grid		Staggered grid
Coupling algorithm		Fractional step method
Time advancement	conductive term	Crank-Nicolson method
	other terms	Adams-Bashforth method
Spatial scheme		2nd-order central difference
Grid points ($x \times y$ (rib outside + rib inside) $\times z$)		$192 \times (96 + 36 \text{ or } 18) \times 96$
Computational volume		$4.8\delta \times 2\delta \times 3.2\delta$

it is assumed that the averaged heat fluxes on both walls, i.e., heat input and output, balance each other. Thus, the temperature on the rough and smooth walls are fixed to T_h and T_c, respectively. The temperature is non-dimensionalized with the temperature difference $\Delta T_w = T_h - T_c$ and then defined as $\theta^* = (T_h - T)/\Delta T_w$. The boundary conditions of the temperature θ^* are as follows:

$$\begin{cases} \theta^* = 0 & \text{(rough wall)} \\ \theta^* = 1 & \text{(smooth wall)} \end{cases} \tag{3}$$

The energy equation governing the thermal field is as follows:

$$\frac{\partial \theta^*}{\partial t^*} + u_j^* \frac{\partial \theta^*}{\partial x_j^*} = \frac{1}{Pr Re_{\tau_0}} \frac{\partial^2 \theta^*}{\partial x_j^* \partial x_j^*}. \tag{4}$$

The calculation conditions are: Reynolds number, $Re_{\tau_0} = 150$; Prandtl number, $Pr = 0.71$, assuming the working fluid to be air. Five types of roughness walls are arranged as listed in Table 2. Case 1 is the similar shape as the experiment of a channel flow with roughness reported by Hanjalić and Launder (1972), and in Case 2 the ribs are set to half the height of Case 1. In Case 3, the height is set to half the height of Case 2. In Cases b and c, the height of the ribs is set the same as in Case 1, though the width of the enclosure is varied systematically. According to the classification of roughness walls (Townsend, 1976), Cases $1 \sim 3$ belong to k-type roughness, where the effect of the roughness is expressed in terms of the roughness Reynolds number, $H^+ = u_\tau H/\nu$; Cases b and c are d-type roughness, where the effect of the roughness cannot be expressed by H^+.

RESULTS AND DISCUSSION

Heat Transfer and Skin Friction Coefficients

Figures 2 and 3, respectively, show the mean skin friction coefficient and the Nusselt number against the Reynolds number. The local skin friction coefficient and the Nusselt number are defined as follows, by taking into account the asymmetry in the flow field disturbed by the ribs:

$$C_f = \frac{\tau_w}{\frac{1}{2}\rho \langle U \rangle^2}, \qquad Nu = \frac{2 q_w d}{(\langle T \rangle - \bar{T}_w)\lambda}, \tag{5}$$

where d indicates the distance between the wall and the location where the Reynolds shear stress becomes zero, and $\langle\ \rangle$ denotes the bulk mean over the distance d. By using Eq. (5), the mean skin friction coefficient, $\overline{C_f}$, and the Nusselt number, $\overline{Nu}$, are defined as the arithmetic mean at both walls. In order to compare the results with the correlation curves by Dean (1978) for the fully-developed channel flow and by Kays and Crawford (1980) for the pipe flow, the length scale of the Nusselt and Reynolds numbers is replaced by equivalent diameter in Figs 2 and 3. The wall shear stress at the (upper) smooth wall is estimated directly by the mean velocity gradient on the wall and that at the (lower) rough wall by calculating the balance of the imposed pressure gradient with wall shear stresses. In those figures, the DNS results in plane channel flow ($Re_\tau = 150$) calculated by the spectral method (Nagano and Hattori, 2003) are also included to compare with the results of the present DNS.

Table 2: Parameters of ribs

	H	W	I	Roughness type
Case 1	0.2δ	0.2δ	0.6δ	k-type
Case 2	0.1δ	0.2δ	0.6δ	
Case 3	0.05δ	0.2δ	0.6δ	
Case b	0.2δ	0.4δ	0.4δ	d-type
Case c	0.2δ	0.2δ	0.2δ	

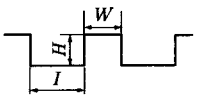

Table 3: Coefficients for heat-transfer rate

	$(\overline{St}/\overline{C_f})/(\overline{St_0}/\overline{C_{f0}})$	$\overline{C_f}/\overline{C_{f0}}$	$\overline{Nu}/\overline{Nu_0}$
Case 1	0.75	1.95	1.58
Case 2	0.77	1.73	1.44
Case 3	1.04	1.24	1.38
Case b	0.69	1.36	1.00
Case c	0.71	1.23	1.04

Table 3 shows the Stanton number [$St = Nu/(Re\,Pr)$], the skin friction coefficient and the Nusselt number, which are divided by the estimated values from the respective correlation curve (Dean, 1978; Kays and Crawford, 1980) for the same Reynolds number. From Fig. 2, even though the imposed pressure gradient is the same as in the smooth wall, the rib decreases the mean velocity, so the Reynolds number strongly depends on the rib configuration; in Case 1, where the rib is the highest in the k-type roughness walls, the Reynolds number is the smallest among them. In all cases, C_f becomes larger than for a smooth wall, so the drag becomes greater. From comparison of the each case, C_f in the k-type roughness becomes larger than that in the d-type roughness; and in each classification, the higher the rib, the more the drag.

On the other hand, the Nusselt number scarcely changes, although the C_f increases in d-type roughness (Cases b and c). Moreover, in the k-type classification, Case 1 enhances heat transfer most. How-

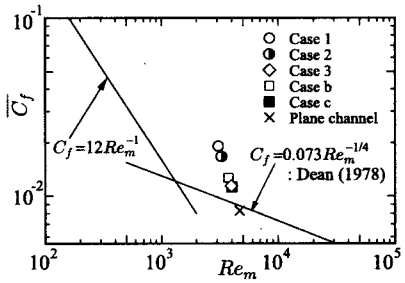

Figure 2: Distributions of skin friction coefficients

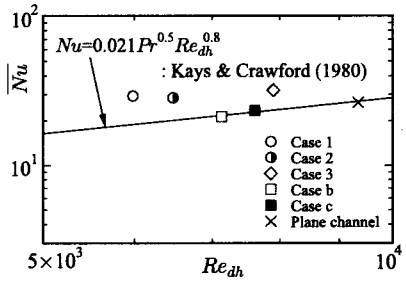

Figure 3: Distributions of Nusselt numbers

ever, from the viewpoint of the heat transfer characteristic including the drag, if we compare the Stanton number divided by the skin friction coefficient $\overline{St}/\overline{C_f}$, from Table 3, Case 1 enhances the heat transfer more than the smooth wall, but the overall characteristics of heat transfer do not improve because of the drag. Therefore, it is concluded that Case 3, the k-type with the lowest ribs, can promote the heat transfer with very low drag. This case is the most efficient from the standpoint of overall heat transfer performance including the drag. Thus, in the following, we discuss the effects of the height of the rib on the statistical characteristics of thermal property in the k-type roughness, which includes a configuration which promotes the heat transfer.

Velocity and Thermal Fields around the Rib

To visualize the velocity and thermal fields around the rib, Figs. 4 and 5 show the mean streamlines estimated from the mean velocity profiles and contour lines of the mean temperature distributions. From the streamlines, the two-dimensional vortices exist in the enclosures between the ribs in Cases 1 and 2. Moreover, their shapes are different in Cases 1 and 2. In Case 1, the center of the two-dimensional vortex is biased to the upstream side of the rib and becomes asymmetric. On the other hand, in Case 2, the center of the vortex is located in the middle of the enclosure. Moreover, in Case 3, the small two-dimensional

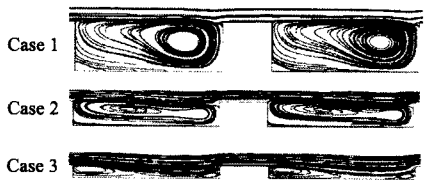

Figure 4: Streamlines of mean velocity

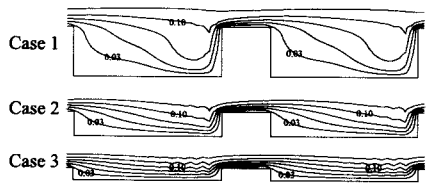

Figure 5: Contour-lines of mean temperature

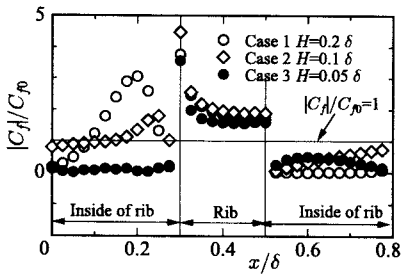

Figure 6: Profiles of local skin friction coefficients around rib

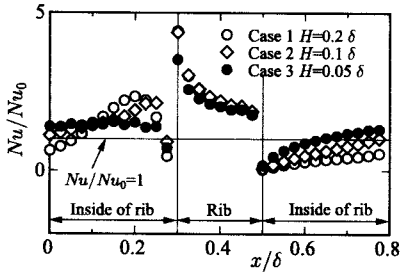

Figure 7: Profiles of local Nusselt number around rib

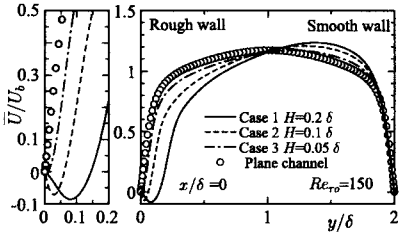

Figure 8: Profiles of mean velocity

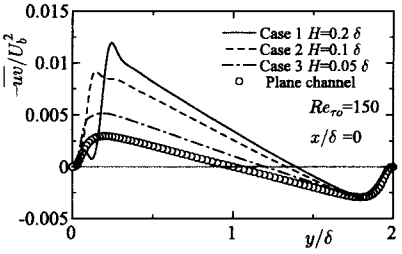

Figure 9: Profiles of Reynolds shear stress

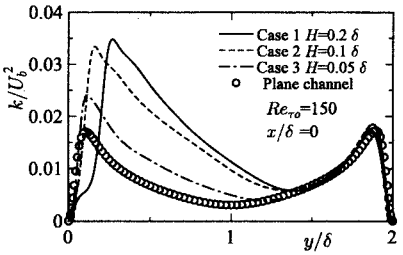

Figure 10: Profiles of turbulence energy

vortices are located both side of the rib, and the reattachment point are seen in the enclosure. The reattachment point is located at $x/\delta = 0.1$ in the enclosure between the ribs.

On the other hand, from the contour lines of the mean temperature, around the front corner of the rib, the spacing between the lines become dense, thus, the heat transfer is very active there. In the enclosure between the rib, the contour lines are distorted corresponding to the streamlines and are not parallel to the bottom wall. Especially, in Case 3, it is confirmed that the mean temperature contour lines are densely distributed, so the heat transfer is more enhanced there.

Figure 6 shows the local skin friction coefficient and the Nusselt number defined by Eq. (5). The local skin friction coefficient increases to take the local peak in the enclosure and the maximum at the front corner of the rib in Cases 1 and 2. On the other hand, in Case 3, although the C_f takes the maximum at the front corner of the rib, there is not a large overall increase in C_f, and the local peak cannot be seen. The local Nusselt numbers in Case 1 and 2 show distributions similar to that of the skin friction coefficients. However, in Case 3, the Nusselt number increases over the entire region in the enclosure. This situation is also observed near the reattachment region of the backward-facing step flows (Vogel and Eaton, 1985), and it is reported that the heat transfer coefficient reaches maximum there. Similarly, the Nusselt number increases in approaching the reattachment point $x/\delta = 0.1$. From the above results, it is confirmed that in Case 3, the heat transfer is promoted, yet with only a relatively small increase in the drag.

Statistical Characteristics of Velocity Field and Turbulent Structures

It is considered that in a velocity field of a channel flow with the rib surface, the flow motions in the enclosure between the rib strongly affect the flow field above the ribs. Thus, in the following, the statisti-

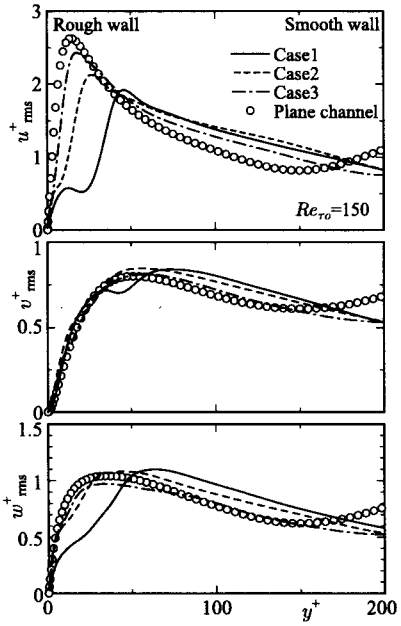

Figure 11: Distributions of turbulent intensities

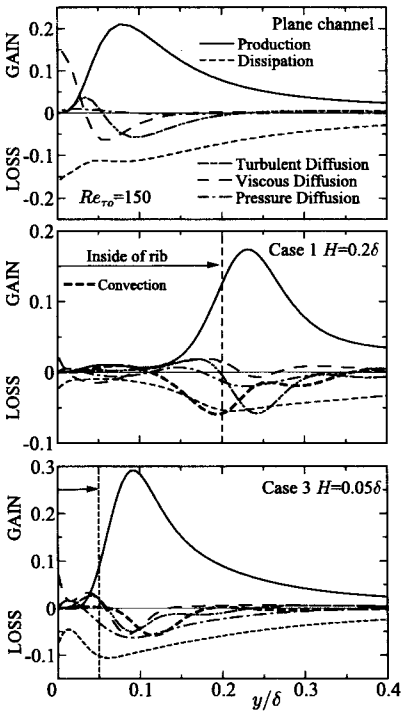

Figure 12: Budgets of turbulence energy

cal quantities of turbulence in the middle of the enclosure ($x/\delta = 0$) are discussed, because the indifferences cannot be seen along the streamwise direction except near the roughness element. As for the k-type roughness, it is well known that the statistical quantities are scaled with the friction velocity. In the present study, the behavior is confirmed in the region above the rib ($y \geq H$).

Figure 8 shows the mean velocity normalized by the bulk velocity U_b. Because of the effects of the rib, it is observed that at the downstream side of the rib, the velocity decreases. In Cases 1 and 2, it can be concluded that the reverse flow in the enclosure is the cause of the increasing drag, as shown in Fig. 4. The corresponding distributions of the Reynolds shear stress and turbulent energy are shown in Figs. 9 and 10. As the rib height increases, the turbulence is promoted, and both the Reynolds shear stress and the turbulence

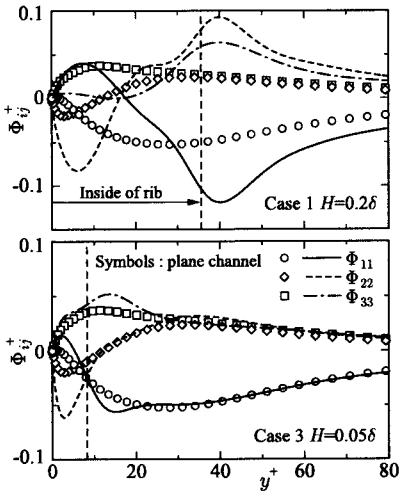

Figure 13: Distributions of pressure strain terms in transport equations of Reynolds stress

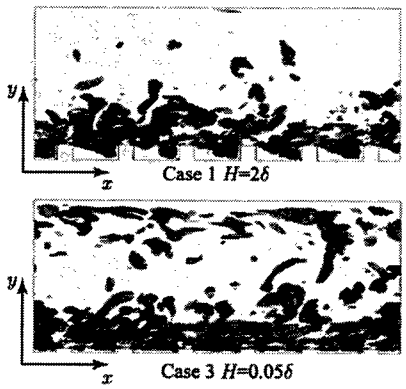

Figure 14: Vortex structures visualized by second invariant: II* $<$ -0.5

energy increase near the wall. This affects the region over the center of the channel. However, in the near-wall region of the opposite wall, no effects are observed, in comparison with the results for the plane channel flow. Despite the negative value of the velocity gradient near the wall in the enclosure as seen in Fig. 8, the Reynolds shear stress takes a positive value, thus confirming the occurrence of counter gradient diffusion. Because the production of the Reynolds shear stress is mainly maintained with the pressure-strain correlation and the pressure diffusion, no production from the mean shear is observed. An experimental study (Hanjalić and Launder, 1972) indicated that the place where the Reynolds shear stress takes zero and the mean velocity becomes maximum is different. However, the difference of these is about 2.8% (0.056δ) per a channel width in the present results. This might be because the Reynolds number studied is relatively small.

Figure 11 shows the turbulence intensities normalized by the friction velocity u_τ on the rough wall. It is observed that in all cases the statistical quantities get together well in the upper region of the ribs. However, from Fig. 10, it is observed that the turbulence intensities relative to the bulk mean velocity increase. To consider the phenomena, the budget of the turbulence energy is shown in Fig. 12. From Case 1, the advection term is enhanced in comparison with the plane channel flow. Because the mean vertical flow component near the rib has occurred, and also because there is a variation in the turbulence in the streamwise direction. Moreover, the contributions from the turbulent and pressure diffusion terms are very high; in the enclosure between the ribs, there is no production from the mean shear, but turbulent transport maintains the turbulence there. This is one of reason for the increase on the rough-wall side. In Case 3, the distribution

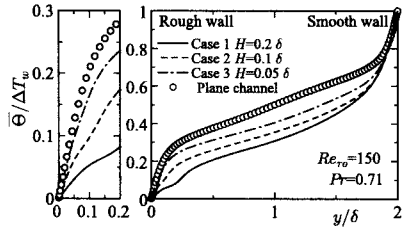

Figure 15: Profiles of mean temperature

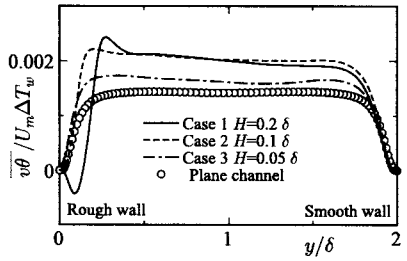

Figure 16: Profiles of wall-normal turbulent heat flux

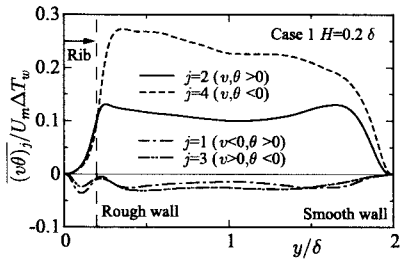

Figure 17: Fractional contributions of organized motions to wall-normal turbulent heat flux

of the budget is similar to the result in the plane channel, in comparison with Case 1, but the contributions from the turbulent transport (turbulent and pressure diffusions) are large.

Next, to investigate the anisotropy of turbulence, Fig. 13 shows the pressure-strain correlation terms which are important in the near-wall region. The pressure-strain correlation is affected because the flow impinges on the upstream side of the wall, and the pressure fluctuations increase over a wide region on the rough-wall side in comparison with the smooth-wall side. If we compare Case 1, where the rib is highest, with the plane channel flow, the respective components of the pressure-strain term become maximum in the region between the ribs, and a very active energy exchange has occurred. In Case 1, the sign of the Φ_{11} becomes positive at $y^+ \sim 15$. As in the wall turbulence without external force, it is observed that in the near-wall region, the splatting effect caused by $\overline{v^2}$ gives the energy to $\overline{w^2}$ as seen in the DNS results (Nagano and Hattori, 2003) included in the figure. However, in the enclosure between ribs, the energy hardly redistributes to the $\overline{w^2}$ component. This is the result of the two-dimensional vortices existing in the enclosure, which promote the redistribution from the $\overline{v^2}$ to $\overline{u^2}$ components. As for Case 3, the effects from the two-dimensional vortex and the reattachment are combined and they affect the redistribution mechanism. This can be considered as the combined result of Case 1 and the plane channel flow. As a result, as shown in Fig. 11, in spite of the existing rough-wall surface, the anisotropy of turbulence shows behavior similar to that in the smooth wall, and the roughness greatly promotes the heat transfer with a relatively small drag.

Finally, Fig. 14 shows the streamwise vortices educed with the second invariant tensors of the velocity gradient II (Kasagi *et al.*, 1995; Iida, Iwatsuki and Nagano, 2000). In each case, the streamwise vortices are produced in the region above the ribs on the rough-wall

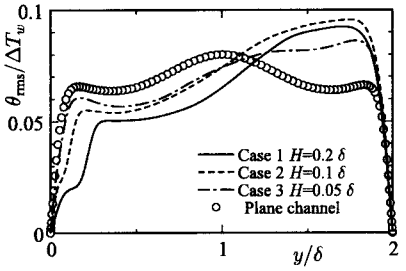

Figure 18: Profiles of temperature variance

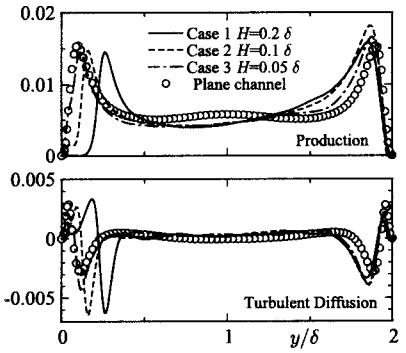

Figure 19: Production and turbulent diffusion terms in budget of temperature variance

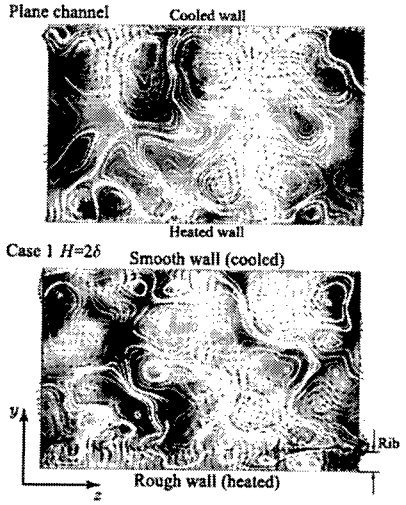

Figure 20: Streamwise-averaged streamlines and temperature fluctuations in $y-z$ plane: $\theta/\Delta T_w = -0.05$ (white)~0.05 (black)

side, and it is confirmed that the structures spread over the region above the center of the channel. Moreover, if we compare Case 1 with Case 3, many more streamwise vortices are produced in Case 1, where the rib effects are strong. In the enclosure between the ribs, the streamwise vortices are seen in the whole region of the enclosure in Case 3. However, in Case 1, because the flow stagnates downstream of the rib surface, not many streamwise vortices are produced. This corresponds to the results of the distributions of skin friction coefficient and Nusselt number as seen in Figs. 6 and 7.

Statistical Characteristics of Thermal Field and Related Turbulent Structures

For the thermal field, the turbulent statistics at the middle of the cross-sectional enclosure ($x/\delta = 0$) are discussed below. Figure 15 shows the mean temperature distribution normalized by the temperature difference ΔT_w. The effect of the rib causes the mean temperature to become asymmetric in all cases as for the mean ve-

locity profiles, and the temperature increases in the major part of the channel. On the other hand, because of the rough-wall side effects, the region of the large temperature gradient extends to the smooth wall side. Figure 16 shows the turbulent heat flux in the wall-normal direction. The heat transfer is activated from the enclosure with the ribs, but in the thermal field also the counter gradient diffusions occur in Case 1. This is because the turbulent heat fluxes are maintained by both the pressure-temperature gradient correlation and turbulent diffusion. However, the production from the mean temperature gradient is not the same as for the Reynolds shear stresses. Moreover, as seen in Fig. 17, in the near-wall region of Case 1, the interaction motions (j=1 and 3) become more active than the ejection (j=2) and sweep motions (j=4); this is why the counter gradient diffusion occurred.

Next, Fig. 18 shows the temperature variances, which decrease on the rough-wall side, where the turbulence of velocity fluctuation are promoted. However, the temperature variances increase on the smooth-wall side, where the turbulent velocity fluctuation is suppressed. The contrary situations occur between the velocity and thermal fields on each side. To investigate the reason why the contrary situations occur, Fig. 19 shows the production and turbulent diffusion terms of the transport equation for $\overline{\theta^2}/2$ in each case. The production terms on the smooth-wall side, where the temperature gradient is large and the wall-normal heat fluxes increase, contributes greatly in the region from the peak place to the center of the channel. This is why the temperature variances become large on the smooth-wall side. On the other hand, on the rough-wall side, because the contribution from the production decreases and the turbulence is maintained by the turbulent diffusion, the intensities of temperature fluctuations decrease, especially in Case 1.

Finally, to observe the spatial structures which contribute to the transport of the passive scalar, Fig. 20 shows the streamlines, which are spatially averaged along the streamwise direction, and the temperature fluctuations in the $y - z$ cross section in the plane channel flows and Case 1. In the plane channel flow, the streamlines show the streamwise vortices in the near-wall region; the mixing of the temperature fluctuations becomes active around the vortices. On the other hand, in Case 1 large-scale vortex structures appear, which extend to the center of the channel from the enclosure between the ribs. With this vortex structure, the turbulent mixing becomes larger in the center of the channel, and the turbulence transport is promoted. This behavior is consistent with the above-mentioned statistical results, i.e., the increase in the heat transfer coefficient, the change in the mean temperature distributions, and the increase in the turbulent diffusion terms, which appear in the budget of temperature variance.

CONCLUSIONS

In this study, in order to elucidate the effects of roughness on the statistical quantities in the velocity and thermal fields, direct numerical simulations (DNS) of heat transfer in turbulent channel flows with transverse-rib roughness have been performed by varying their spacing, width and height. The results are summarized as follows.

1. The Reynolds number differs greatly with the ribs arrangement, because of the decrease in the mean velocity, although the pressure gradient is identical with the plane channel flow. For the k-type roughness, heat transfer is promoted by increasing the height of the ribs, , but at the same time, the drag increases. This results in a deterioration in heat transfer efficiency compared with the smooth wall flow. However, with decreasing rib heights, the heat transfer performance can be promoted with a small increase in drag, and the heat transfer characteristic improves. This phenomenon is not observed with d-type roughness.

2. Because the flow impinges upstream of the rib, the pressure fluctuation becomes larger in the wide region of the rough wall side. In this situation, turbulence is maintained in the enclosure between the ribs. Also, counter-gradient diffusion is observed for the Reynolds shear stress and the wall-normal heat fluxes, and it is confirmed that this results from pressure-related transport terms.

3. In the enclosure between ribs low in height, the streamwise vortices are seen over the entire region in the enclosure; when the ribs are high, however, the flow stagnates downstream of the ribs and streamwise vortices are not produced. Thus, the local Nusselt number decreases from downstream of the ribs to the center of the enclosure. Moreover, the skin friction coefficient increases because of the effects of the streamwise vortices, which are seen above the ribs, while the local Nusselt number does not increase. As a result, the total heat transfer characteristics including the drag deteriorate.

4. Because the higher the rib, the large scale vortices appear in the center of the channel from the enclosure between the ribs, the turbulent mixing is enhanced and the mean heat transfer coefficient increases, but the drag also increases. Therefore, by arranging so that ribs will be lower in height and having the mixing occur in the near-wall region, the overall heat transfer performance becomes much effective including the drag.

ACKNOWLEDGEMENT

The authors gratefully acknowledge the support provided for this research by the New Energy and Industrial Technology Development Organization (NEDO) through the Japan Weather Association.

REFERENCES

Antonia, R. A., and Luxton, R. E., 1971, "The Response of a Turbulent Boundary Layer to a Step Change in Surface Roughness Part 1. Smooth to Rough", *J. Fluid Mech.*, Vol. 48, pp. 721–761.

Antonia, R. A., and Luxton, R. E., 1971, "The Response of a Turbulent Boundary Layer to a Step Change in Surface Roughness Part 2. Rough to Smooth", *J. Fluid Mech.*, Vol. 53, pp. 737–757.

Dean, R. B., 1978, "Reynolds Number Dependence of Skin Friction and Other Bulk Flow Variables in Two-Dimensional Rectangular Duct Flow", *Trans. ASME, J. Fluid Engng.*, Vol. 100, pp. 215–223.

Hanjalić, K., and Launder, B. E., 1972, "Fully Developed Asymmetric Flow in a Plane Channel", *J. Fluid Mech.*, Vol. 51, pp. 301–355.

Iida, O., Iwatsuki, M., and Nagano, Y., 2000, "Vortical Turbulence Structure and Transport Mechanism in a Homogeneous Shear Flow", *Phys. Fluids*, Vol. 12, pp. 2895–2905.

Kasagi, N., Sumitani, Y., Suzuki, Y., and Iida, O., 1995, "Kinematics of the Quasi-Coherent Vortical Structure in Near-Wall Turbulence", *Int. J. Heat and Fluid Flow*, Vol. 16, pp. 2–10.

Kays, W. M., and Crawford, M. E., 1980, *Convective Heat and Mass Transfer*, 2nd ed., McGraw-Hill, pp. 323–325.

Nagano, Y., and Hattori, H., 2003, "DNS and Modelling of Spanwise Rotating Channel Flow with Heat Transfer", *Journal of Turbulence*, Vol. 4, in press.

Perry, A. E., 1969, "Rough Wall Turbulent Boundary Layers", *J. Fluid Mech.*, Vol. 37, pp. 383–413.

Townsend, A. A., 1976, *The Structure of Turbulent Shear Flow*, 2nd ed., Cambridge Univ. Press, pp. 139–143.

Tsujimoto, K., Miyake, Y., and Nakaji, M., 2000, "Direct Numerical Simulations of Rough-wall Heat Transfer in a Turbulent Channel Flow", *Proc. 3rd Int. Symposium on Turbulence, Heat and Mass Transfer* (Nagano et al., eds), Aichi Shuppan, pp. 175–182.

Vogel, J. C., and Eaton, J. K., 1985, "Combined Heat Transfer and Fluid Dynamic Measurements Downstream of a Backward-Facing Step", *Trans. ASME, J. Heat Transfer*, Vol. 107, pp. 922–929.